# Fully Porous GaN p−n Junction Diodes Fabricated by Chemical Vapor Deposition

Oleksandr V. Bilousov,[†] Joan J. Carvajal,*[,†] Hugh Geaney,[‡,∥] Vitaly Z. Zubialevich,[∥] Peter J. Parbrook,[∥,§] Oscar Martínez,[⊥] Juan Jiménez,[⊥] Francesc Díaz,[†] Magdalena Aguiló,[†] and Colm O'Dwyer*[,‡,∥]

[†]Física i Cristal·lografia de Materials i Nanomaterials (FiCMA-FiCNA) and EMaS, Universitat Rovira i Virgili (URV), Marcel·lí Domingo s/n, E-43007 Tarragona, Spain

[‡]Department of Chemistry and [§]School of Engineering, University College Cork, Cork, Ireland

[∥]Tyndall National Institute, Lee Maltings, Dyke Parade, Cork, Ireland

[⊥]GdS-Optronlab, Departamento Física Materia Condensada, Univ. de Valladolid, Edificio I+D, Paseo de Belén, 11, 47011 Valladolid, Spain

**Ⓢ** *Supporting Information*

**ABSTRACT:** Porous GaN based LEDs produced by corrosion etching techniques demonstrated enhanced light extraction efficiency in the past. However, these fabrication techniques require further postgrown processing steps, which increases the price of the final system. Also, the penetration depth of these etching techniques is limited, and affects not only the semiconductor but also the other elements constituting the LED when applied to the final device. In this paper, we present the fabrication of fully porous GaN p−n junctions directly during growth, using a sequential chemical vapor deposition (CVD) process to produce the different layers that form the p−n junction. We characterized their diode behavior from room temperature to 673 K and demonstrated their ability as current rectifiers, thus proving the potential of these fully porous p−n junctions for diode and LEDs applications. The electrical and luminescence characterization confirm that high electronic quality porous structures can be obtained by this method, and we believe this investigation can be extended to other III−N materials for the development of white light LEDs, or to reduce reflection losses and narrowing the output light cone for improved LED external quantum efficiencies.

**KEYWORDS:** *porous GaN, porous p−n junction diode, light emitting diodes, chemical vapor deposition, epitaxial growth*
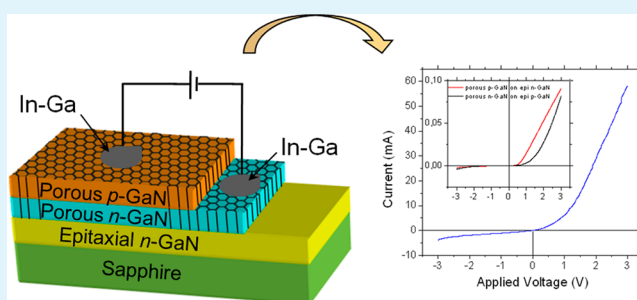
## 1. INTRODUCTION

Modern society is experiencing an ever-increasing demand for energy to power a vast array of electrical and mechanical devices. A significant amount of the energy consumed is for lighting purposes. For instance, this demand is ∼17% of the total energy consumed in the U.S.A. in 2011.[1,2] Thus, any approach that can reduce energy consumption is important. In this context, the development of light emitting diodes (LEDs) incorporating at least one porous component, with improved light extraction efficiency, is being explored intensively.[3−13] However, up to now, only partially porous p−n junctions have been analyzed for this purpose.

The overall efficiency of an LED is mainly determined by internal quantum efficiency and light-extraction efficiency.[8] The internal quantum efficiency ($\eta_{int}$) is the number of photons generated from an electron−hole pair injected into QWs, that is, the ability of the semiconductor LED to convert electricity into light.[12] Because of the lack of lattice-matched substrates, a number of lattice defects such as dislocations and vacancies are formed during the epitaxial growth, which causes a large decrease in $\eta_{int}$ of GaN LEDs.[8] One way to improve $\eta_{int}$ is to enhance the quality of the material. The light-extraction efficiency ($\eta_{ex}$) is another important parameter that should be improved, representing the ability of efficiently extracting the generated light from within the semiconductor to the outside ambient.[12] In planar LEDs, $\eta_{ex}$ is limited by the total internal reflection at the interface of the semiconductor and outer media. Because the difference between refractive indices of GaN ($n_{GaN}$ = 2.5 at 460 nm)[12] and air ($n_{air}$ = 1) is large, the total internal reflection confines the generated luminescence mostly inside the LED cavity,[3] and as much as 18% of light is reflected back into the semiconductor at normal incidence[12] and is reabsorbed by the LED.[11] The critical angle of total internal reflection is 23.6° for GaN,[8] which allows only a small fraction of the light generated in the active layer of the LED to escape into the surrounding environment.

Roughening the surface, or generating a porous structure, might diminish the total internal reflection of the device by

introducing a scattering medium, in which the mean free path for transport of light ($I$) is given by[3]

$$l = 1/\rho\sigma \qquad (1)$$

in which $\rho$ denotes the density of scatterers (related to pore density) and $\sigma$ denotes the cross section for scattering (size of the pores), and attains a maximum when the pore and the wavelength of scattered light have comparable dimensions. So then, multiple scattering of photons in porous structures results in an enhanced light extraction of the LED.[11] Also, the light emitted from the active layer of the LED is deflected by the porous layer, and thus, the porous structure minimizes the total internal reflection an increases the transmission at the interface to air, since the effective refractive index ($n_{eff}$) of the porous structure is reduced when compared to that of the bulk semiconductor. This allows for the reduction in optical losses due to Snell and Fresnel transmission[14,15] and a decrease in the total internal reflection enlarging the light extraction cone, contributing to the increase on the light extraction efficiency.[16] Furthermore, the porous structure also generates an angular randomization of the photons since multiple interfaces with different orientations exists in which Snell's law can be accomplished.[17] Finally, it is also worth pointing out that porous structures have been reported to be responsible also for an increase of the internal quantum efficiency due to the geometrical quantum wire effect associated with the thin walls remaining between the pores.[18]

Despite the wide interest of porous semiconductors in view to their peculiar electrical, optical, and mechanical properties for applications in many fields, from electronics to optoelectronics,[19−21] from photovoltaics[22] to biomedicine and environment monitoring,[23,24] fabrication of totally porous p−n junctions has been scarcely investigated and restricted almost exclusively to porous Si or III−Vs produced by anodization. The rectifying behavior of entirely porous p−n junctions is, from a theoretical point of view, compatible with that of a high-density of randomly distributed elemental mesoscopic p−n crystalline junctions operating in parallel.[25] Also, it has been pointed out that conventional planar nonporous diode structures exhibit a number of inherent deficiencies that result in relatively low energy-conversion efficiencies, a problem that might be overcome by completely porous p−n junctions.[26] In fact, a 10-fold enhancement of efficiency compared to that of the usual planar nonporous devices has been demonstrated for totally porous Si p−n junctions in betavoltaics, and it has been postulated that significant efficiency gains might be expected also in photodetectors and solar cells fabricated using completely porous p−n junctions.[26] InGaN-based solar cells are attractive since their direct and tunable bandgaps might span nearly the full solar spectrum, with a theoretical efficiency over 40%, and with superior radiation resistance for operation under harsh environments.[27] Porous p−n junctions might be useful in this case to prevent the optical losses at the interfaces of these solar cells, arising from the abrupt change of refractive indexes between air and the device. Thus, these porous structures can act as an antireflection layer with increased internal multiple reflections, if the size of the pores is larger than the incident wavelength, or with a gradient change of the refractive index from air to the device, if the geometric features of the structure are smaller than the incident wavelength, which in both cases will contribute to enhance the efficiency of InGaN-based solar cells.[28]

The use of fully porous p−n junctions might be especially important for enhancing the light extraction of LEDs and solar cells. It has been demonstrated that the induction of a porous structure in the LED device can lead to an enhancement of the light extraction efficiency of the device.[3] In fact, the induction of partially porous p−n junctions in GaN-based LEDs has led to different improvements of the light extraction efficiencies. For instance, an increase of 12% of the internal quantum efficiency and 23% higher optical power has been reported on a GaN diode including a photonic crystal structure in its n-type component,[8] while an increase by 70% on the optical output power has been demonstrated for a LED with a photonic crystal structure selectively grown on p-type GaN.[11] Using nanotextured p-type GaN, a 46% higher light output than in a standard LED with unpatterned p-type GaN has been reported.[12] Furthermore, it has been postulated that if the porous structure, forming a photonic crystal structure, crosses the active region of the LED (i.e., the p−n junction thus forming an entirely porous p−n junction), the increase in light extraction efficiency could be enhanced even further.[4] A light output power improvement as high as 94% has been demonstrated for such structures fabricated by chemical etching, in which porosity affected even the ITO electrode.[13] In the case of solar cells, a giant efficiency enhancement by up to 146% as compared with planar surfaces has been reported in InGaN solar cells combining a hierarchical surface texture as the antireflection layer.[28]

Recently, we have demonstrated that it is possible to produce nanoporous GaN by crystal growth methods during chemical vapor deposition (CVD), and without the need of any postgrowth treatment to induce porosity.[29,30] We have also demonstrated that we can produce both n-type and p-type porous GaN by this methodology with a high density of charge carriers ($\sim 10^{18}$ cm$^{-3}$) and even forming low resistivity Ohmic contacts with high work function metals such as Au or Pt.[31,32]

In this paper, we present the fabrication of fully porous p−n junctions by using nanoporous GaN produced by CVD, and compare their performance with partially porous p−n junctions fabricated using the same methodology, in which only the n-type or p-type GaN layers are porous. We characterized their diode behavior at high temperatures, and demonstrated their ability as current rectifiers, thus proving the potential of these fully porous p−n junctions for diode and LEDs applications.

## 2. EXPERIMENTAL SECTION

### 2.1. Fabrication of Partially and Totally Porous GaN Diodes.

Nanoporous GaN thin layers were grown on commercial nonporous GaN thin films with complementary electrical conductivity produced on sapphire (0001) substrates. The porous films were grown by the direct reaction of metallic Ga with ammonia in a tubular CVD system, using gallium metal (99.999%) and ammonia (99.99%), as Ga and N sources, respectively. To produce porous p-type GaN, Mg was introduced in the furnace in the form of magnesium nitride (99.95%), placing it 4 cm upstream of the Ga source. The substrate was placed 1.7 cm above the Ga source. Prior to their introduction in the furnace, the substrates were cleaned with ethanol. When the substrate and the Ga and Mg precursors were introduced in the furnace, the quartz tube of the furnace was degassed to a vacuum pressure of $1 \times 10^{-2}$ Torr. Ammonia was then introduced through a mass-flow controller at a flow rate of 75 sccm, while the pressure was set at 15 Torr and the furnace was heated up to the reaction temperature of 1203 K. Then, the furnace was kept at constant temperature for 60 min under constant $NH_3$ flow and pressure, while the chemical reaction took place. When the reaction was finished, the furnace was cooled down to room temperature while the ammonia flow was stopped; thus, the
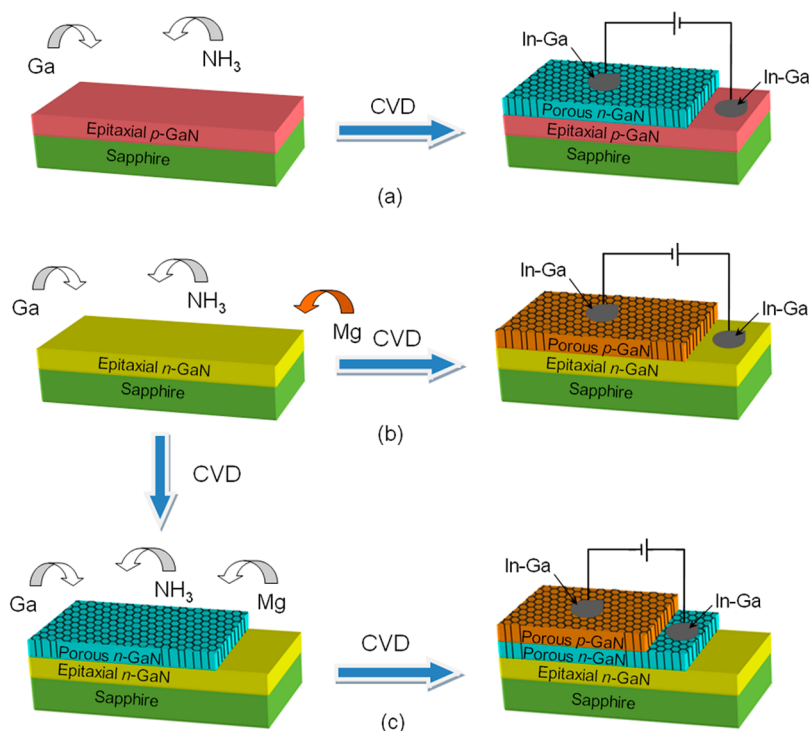
**Figure 1.** Schematic representation of the formation process of partially and fully porous GaN p−n junctions by CVD: (a) undoped n-type porous GaN on nonporous p-type GaN, (b) Mg-doped porous p-type GaN on nonporous n-type GaN, and (c) Mg-doped porous p-type GaN on undoped porous n-type GaN.

pressure of the system dropped to $1 \times 10^{-2}$ Torr. After growth, the samples containing porous Mg-doped GaN were annealed at 973 K in $N_2$ atmosphere for 20 min in order to break Mg−H complexes and activate the p-type conductivity in porous GaN. The different porous layers were produced by selective-area growth by placing a BN mask in close contact to the substrate to avoid the deposition of the growing layers on the outer parts of the substrate or the previously grown porous layer and preserve these regions for later electrical contacting.

**2.2. Morphological and Structural Characterization of Porous GaN.** Nanoporous GaN layers deposited on GaN (0001) substrates were characterized morphologically using a JEOL JSM 6400 scanning electron microscope (SEM). Rocking curves were recorded using a Bruker-AXS D8-Discover diffractometer equipped with parallel incident beam (Göbel mirror), a vertical $\theta-\theta$ goniometer, a XYZ motorized stage and a General Area Diffraction Detection System (GADDS). Samples were placed directly on the sample holder and the area of interest was selected with the aid of a video-laser focusing system. The X-ray diffractometer was operated at 40 kV and 40 mA to generate Cu K$\alpha$ radiation. The GADDS detector was a HI-STAR (multiwire proportional counter of $30 \times 30$ cm$^2$ with $1024 \times 1024$ pixels). The rocking curves covered an omega angle of 6°, collected through 120 frames at a step size of 0.05° and 15 s of exposition time per frame.

**2.3. Cathodoluminescence and Photoluminescence Characterization.** CL measurements were carried out in monoCL2 system from Gatan attached to a field emission scanning electron microscope (FESEM) (Carl Zeiss-LEO 1500) operating at 10 kV. The measurements were carried out at 80 K. The detection for panCL images was done with a photomultiplier tube (PMT), and the CL spectra were recorded with a Peltier cooled charge coupled device (CCD) detector. PL was collected exciting the samples with the 244 nm line (second harmonic of 488 nm line) from a cw Ar-ion laser with a power density of 2 W/cm$^2$. PL spectra were acquired using a Horiba iHR320 spectrometer equipped with a Synapse CCD matrix. Samples were placed in an evacuated chamber of a Janis closed-cycle helium cryostat for temperature-dependent PL measurements.

**2.4. Electrical Characterization.** Two point electrical measurements of partially and totally porous GaN diodes were conducted using In/Ga liquid eutectic contacts and a Biologic SP-50 potentiostat. An In/Ga eutectic droplet was placed on top of the porous GaN material with the other contact placed directly on the nonporous epitaxial n- or p-type GaN, in the case of the partially porous diodes, or on the porous n-type GaN layer, in the case of the totally porous diode. Linear voltage sweeps were obtained in the range between −3 and 3 V with a 50 mV/s sweep rate and of −10 and 10 V with a 50 mV/s sweep rate for temperature-dependent measurements. Diode rectification measurements were conducted in the range between ±0.4 V and ±5 V voltages for forward and reverse bias. The measurements were repeated with contacts on various points of each sample to ensure repeatability.

## 3. RESULTS AND DISCUSSION

**3.1. Crystal Growth and Morphological Characterization.** Epitaxial nanoporous GaN thin layers were grown by CVD through the direct reaction of metallic Ga with ammonia in a tubular reactor on nonporous GaN (0001) thin films (∼3 $\mu$m thick) grown by metalorganic vapor phase epitaxy (MOVPE) on sapphire (0001) substrates. After degassing the quartz reactor to a vacuum pressure of $1 \times 10^{-2}$ Torr, ammonia was introduced through a mass-flow controller at a flow rate of 75 sccm, while the furnace was heated to 1200 K. The growth lasted for 30 min at the constant flow of $NH_3$ and temperature. After growth, the furnace was cooled to room temperature and the $NH_3$ flow was stopped, reducing the pressure inside the reactor to $1 \times 10^{-2}$ Torr. Figure 1 shows a schematic description of the process. We used either n-type or p-type nonporous GaN (0001) thin films deposited on sapphire (0001) as substrates, depending on the experiment and the p−n junction to be formed (Figure 1a,b). Mg-doped samples were grown to produce p-type nanoporous GaN films (Figure 1b). These samples after growth were annealed in a $N_2$ atmosphere
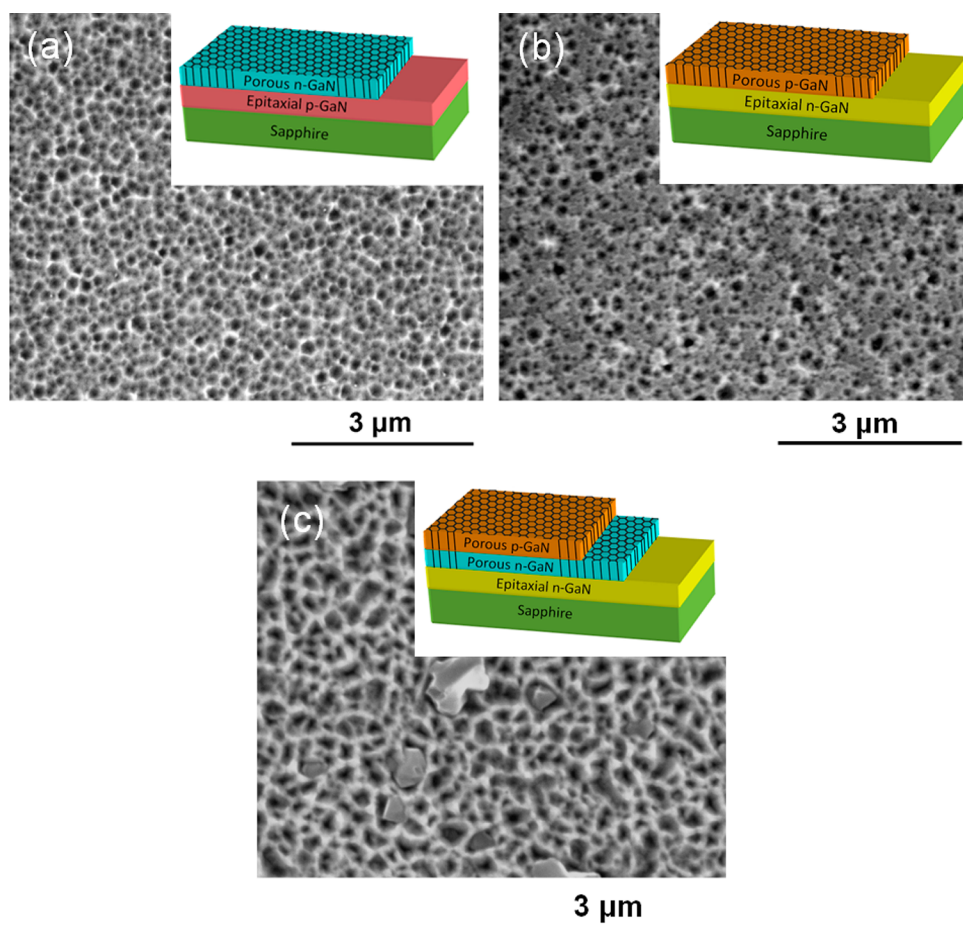
**Figure 2.** (a) Porous n-type GaN grown on nonporous epitaxial p-type GaN, (b) porous p-type GaN grown on nonporous epitaxial n-GaN, and (c) porous p-type GaN grown on porous n-type GaN corresponding to the fully porous diode. Insets show schemes of the structure of the partially and fully porous diodes.

at 973 K for 20 min in order to break the existing Mg−H complexes and activate the p-type conductivity of the porous GaN layers.[33] Fully porous p−n junctions were fabricated in a two crystal growth step process (Figure 1c). First, an undoped n-type porous GaN layer was grown on nonporous GaN(0001). Second, another porous Mg-doped p-type GaN layer was grown on the top of the porous n-type GaN layer as represented in Figure 1, under the same reaction conditions.

In this way, three types of porous GaN diodes were prepared: (i) undoped n-type porous GaN on nonporous p-type GaN (hereafter porous n−p diode), shown schematically in Figure 2a; Mg-doped porous p-type GaN on nonporous n-type GaN (hereafter porous p−n diode), shown schematically in Figure 2b; and Mg-doped porous GaN on undoped porous n-type GaN (hereafter fully porous p−n diode), shown schematically in Figure 2c.

Figure 2 shows also top-view SEM images of the porous GaN layers. All porous GaN layers reveal a high degree of porosity with a large number of pores. Despite being grown under the same conditions, the porous p-type layers tend to show larger diameter pores when compared to those observed on the n-type porous layers. This is especially significant for fully porous GaN p−n diodes. The pores observed in the p-type layer are significantly wider than those on the n-type layer prior to the second growth step that might be related to the corrugation of pores due to a lower decomposition temperature of Mg-doped GaN,[34] which would be accentuated by the presence of the

pores. High magnification images of the porous structures for n-type and p-type GaN layers can be seen in Figure S1 in Supporting Information.

In all cases, however, the porous GaN layers are grown oriented along the c-crystallographic direction, matching the crystallographic orientation of the nonporous epitaxial GaN thin-films used as substrates. Pore hollows are always parallel to this direction.

**3.2. Structural Characterization.** X-ray rocking curves corresponding to the (0004) reflection were used to analyze the influence of structural strain on porous GaN p−n junction diodes, as shown in Figure 3. Figure 3a shows the rocking curves corresponding to the porous n−p diode and defines the response of the epitaxial p- and n-type GaN substrate for comparison, with fwhm of 1541″ and 1508″ for the nonporous and porous layers, respectively, indicating a good orientation of the porous material along the c-crystallographic direction and that the crystalline quality of the porous layer is comparable to the nonporous film, or even better. The peak positions are 72.902° and 73.082° for the nonporous and porous layers, respectively, indicating a slight relaxation of the porous layer when compared to the nonporous one. The magnitude of the relaxation can be estimated according to the following expression:[35]

$$\Delta \in_{\perp} = (c_{strained} - c_{relaxed})/c_{relaxed} \qquad (2)$$
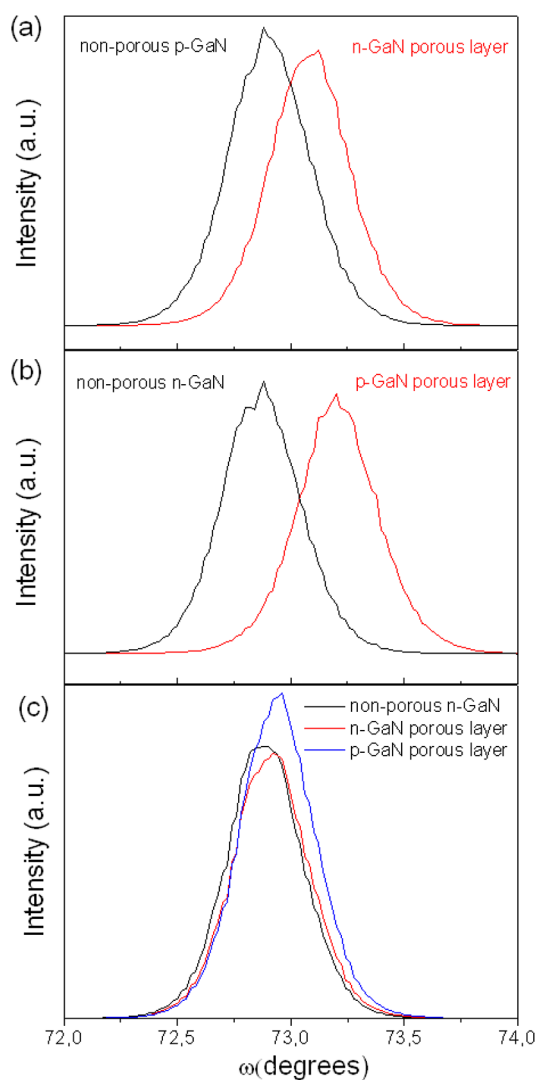
**Figure 3.** Rocking curves of (a) the porous n−p, (b) porous p−n, and (c) fully porous diodes.

were $c_{strained}$ and $c_{relaxed}$ are the $c$ crystallographic parameters of the nonporous p-type and porous n-type GaN layers, respectively, determined from the rocking curves. Accordingly, a reduction of the strain along the $[0001]$ direction of 0.24% was estimated, which stems from the benefit of internal porosity (for details, see Table S1, Supporting Information).

Figure 3b shows the rocking curves corresponding to the porous p−n diode. The relaxation of the p-type porous layer is 0.46%, almost twice that achieved in the porous n−p diode, indicating the beneficial strain relief offered by the porous subsurface.[36] In that case, fwhm is slightly higher for the porous layer but of the same order of that obtained for the nonporous layer, indicating that the crystalline quality of these two films is similar. The relaxation of the porous p-type layer is larger than the one observed for the porous n-type layer, which might be related to the wider size of its pores (see Figure 2b), giving additional compliance to the layer to accommodate on the substrate.

Finally, the fully porous GaN diode exhibits equal fwhm in their rocking curves for the two porous layers and of the same order to that of the nonporous n-type GaN film (see Figure 3c and Supporting Information Table S1). Thus, the crystalline quality of the three films is closely similar. The relaxation

calculated for these porous layers is 0.04% for the n-type porous layer grown on the nonporous n-type GaN film, while that of the p-type porous layer grown on the porous n-type layer is 0.07%. In both homo and heterojunctions, relaxed porous layers are epitaxially grown on either porous or continuous thin films. The minimum strain is found between the nonporous and the porous n-type GaN layers.

**3.3. Cathodoluminescence.** Figure 4 shows SEM and panchromatic cathodoluminescence (panCL) images, as well as CL spectra recorded for all the layers forming the fully porous p−n diode. The SEM image of the nonporous n-type GaN film shows a smooth surface, while the panCL image shows the typical granular luminescence pattern of GaN, due to the distribution of clusters of dislocations in the material.[37,38] The CL spectrum recorded for this layer shows the near-band gap emission (NBE) located at ∼355.6 nm and a donor−acceptor pair (DAP) luminescence at ∼377 nm, which characteristically results from point defects and/or impurities.[39]

The panCL image of the porous n-type GaN layer shows a different distribution of the luminescence emission, which could be related to the porous morphology, even if there is not a full correlation between the pores revealed in the SEM image and the panchromatic image contrast (see Figure 4b). The spectrum recorded for this layer exhibits quite a broad NBE luminescence, corresponding to n-type GaN, peaking at ∼362 nm. A yellow luminescence (YL) band centered at ∼580 nm, normally attributed to point defects (Ga vacancies) and/or impurities, such as oxygen and carbon[40] is also present.

Figure 4c shows the SEM and the corresponding panCL image of the top layer of the fully porous p−n diode (porous p-type GaN). The pores are not visible in the panCL image, similar to what is observed in the porous n-type layer. High intensity regions correspond to porous GaN micron-size particles that grow on the top of porous layer but with a different crystallographic orientation. The CL spectra shown in Figure 4e correspond to the high and low intensity emission regions observed in the panCL image, with the NBE of GaN at ∼358 nm, the DAP band at ∼379 nm and a longitudinal optical (LO) phonon replica at ∼388 nm. These features correspond to the typical CL spectrum of p-type GaN. The spectrum recorded in the high intensity region, corresponding to a GaN micron-size particle grown on the porous layer, has a much lower DAP intensity emission relative to the NBE emission. This effect is likely related to a different Mg doping incorporation of the GaN porous layer and GaN micron-size particles[41] or to a different crystallographic orientation of the two regions,[42] which can also be responsible for changes in the incorporation of the Mg impurities.

SEM and corresponding panCL cross-section images of the totally porous p−n diode were recorded, as shown in Figure 5. The cross-sectional SEM micrograph clearly shows the nonporous GaN film and the porous GaN layers grown by CVD. In the panCL image, the dark lines observed in the nonporous GaN correspond to the threading dislocations crossing the substrate layer. The thickness of the porous GaN layers determined from SEM is ∼2.1 $\mu$m, corresponding to the two porous layers, the Mg-doped porous p-type GaN and the undoped porous n-type GaN layer, each with a thickness of ∼1 $\mu$m. Although the interface between these two porous layers is less discernible in the SEM image, it appears clear in the panCL image, where porous n-type GaN appears dark while porous p-type GaN appears bright. This can be related to a higher concentration of charge carriers in the Mg-doped porous p-type
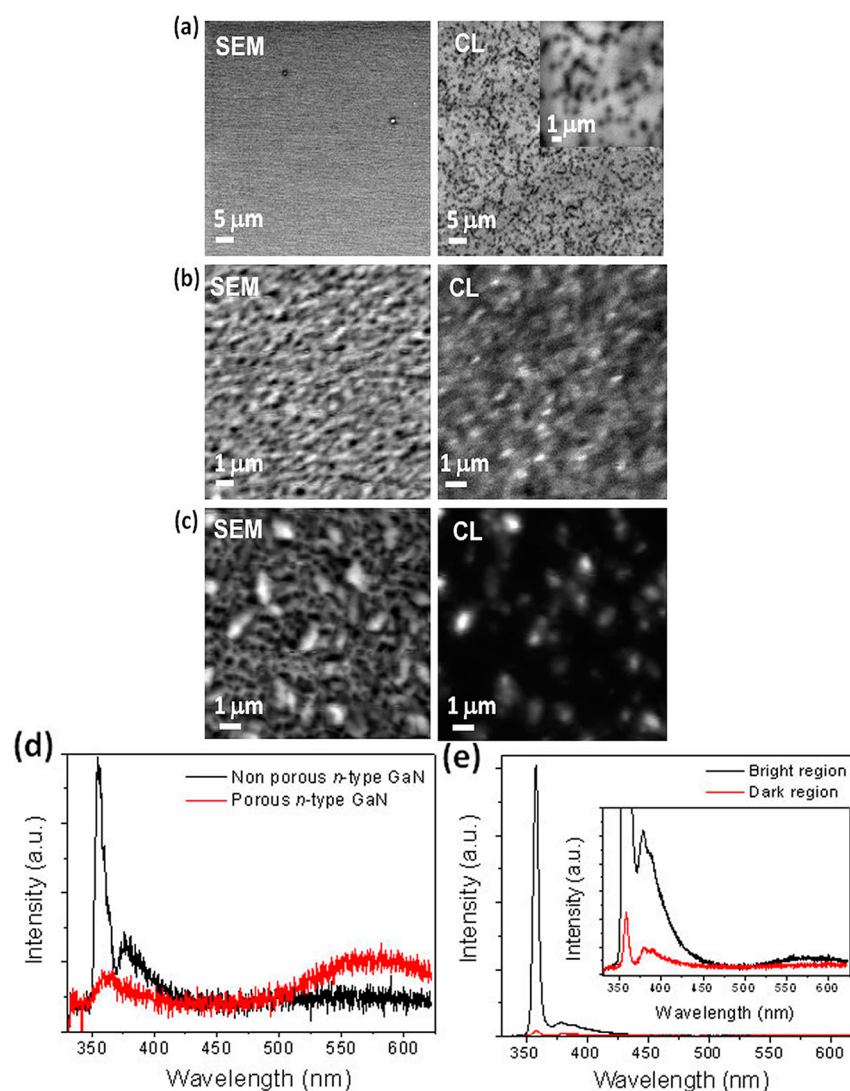
**Figure 4.** Top-view SEM and panCL images taken in the same region of the sample of (a) nonporous n-type GaN film, (b) porous n-type GaN layer and (c) porous p-type GaN, corresponding to the fully porous p−n diode. Insets show magnified areas of the pictures. CL spectra recorded for (d) nonporous and porous n-type GaN, and (e) bright and dark areas observed in the panCL image shown in (c). Inset in the graph is a magnification of the same spectra to show the features observed in the two spectra.

GaN layer ($\sim10^{18}$ cm$^{-3}$) when compared to the undoped porous n-type GaN ($\sim10^{16}$ cm$^{-3}$), as previously consigned.[31,32] The thickness of the two porous layers is proved to be similar in the panCL image. Figure 5c shows the CL spectra recorded for the different layers in the cross section view. In the case of the nonporous n-type GaN film, a strong emission at ∼355 nm is observed similar to the one recorded in top-view (see Figure 4a). In the case of porous p-type GaN only the DAP emission related to the Mg doping is observed, with no emission from NBE, indicative of the incorporation of substitutional Mg for an efficient p-type doping of this layer. The difference with the CL spectrum recorded in top-view (see Figure 4e) indicates that, in that case, the NBE emission observed in the porous layer really arises from the nonporous GaN substrate. Concerning the porous n-type GaN layer, nearly no CL signal was detected, in agreement with the low intensity detected in the top-view configuration (see Figure 4d). The appearance of the yellow band, not observed for the nonporous substrate, confirms that the cross-sectional spectrum corresponds to the porous layer.

**3.4. Photoluminescence.** Photoluminescence (PL) measurements in top view were also performed on both Mg-doped porous GaN and undoped porous GaN layers corresponding to the totally porous GaN p−n junctions at different temperatures from 11 to 300 K at a constant laser power density. Figure 6a shows PL spectra for undoped porous GaN. It exhibits the expected band-edge luminescence with a Varshni-like temperature redshift[43] from 3.43 eV at 300 K to 3.46 eV at 11 K and a narrow fwhm of ∼12 meV at 11 K. Broad emission near the band gap typically results from the density of states tailing due to randomly distributed impurities. This broad emission near-band gap and band-edge emission equilibrate in intensity at 100 K and the broad emission near-band gap slightly dominates at 120 K. However, the band-edge emission dominates at other temperatures.

Figure 6b shows PL spectra for the Mg doped porous GaN. The room temperature band-edge emission appears at lower energy (3.41 eV) when compared to the undoped porous GaN. At temperatures down to 11 K, however, this emission is blue-shifted and located at a value of 3.46 eV with a narrow fwhm of
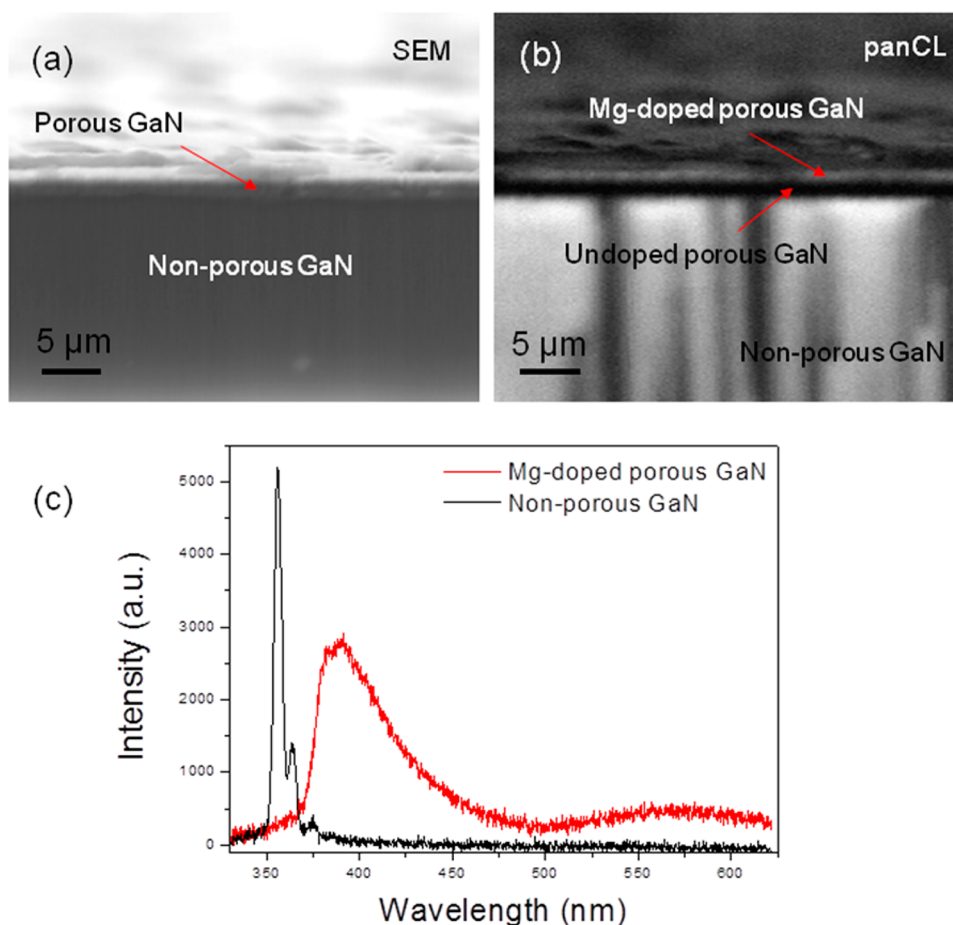
**Figure 5.** (a) Cross-sectional SEM and (b) corresponding panCL images of the fully porous GaN diode. (c) CL spectra recorded for nonporous GaN and Mg-doped porous GaN.
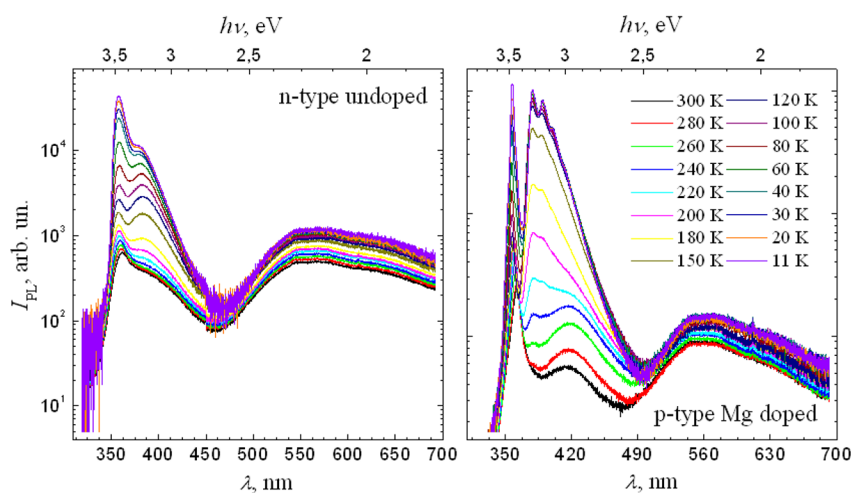


**Figure 6.** Temperature-dependent PL spectra of undoped (a) and Mg-doped GaN (b) porous layers corresponding to the fully porous GaN p−n junction ($\lambda_{ex}$ = 325 nm).

~5 meV. The band gap emission in both undoped and Mg doped GaN is over an order of magnitude more intense at 11 K as compared to room temperature. We observe some structure in the high energy side, at ~3.5 eV, probably associated with a bound exciton.[44] As the GaN is Mg doped and no Si nor shallow O donor-bound excitons are expected to be incorporated in the samples according to the synthesis conditions, we attribute this weak emission to excitons bound

to Mg acceptors. The band-edge luminescence is followed by the DAP luminescence, located at 3.27 and 3.28 eV at 150 and 11 K, respectively. The DAP emission disappears at high temperatures. As expected from Mg acceptors in doped GaN, we find the LO phonon replicas at 3.18 and 3.19 eV at 150 and 11 K, respectively, with several harmonics observable at 11 K indicating the good electronic quality of the p-type porous GaN layer obtained by CVD.[45] Another broad band at ~420 nm

(blue band) is also clearly observed at 300 K, disappearing as the temperature decreases (~200 K). This type of emission has been previously observed[46] and attributed to the formation of a Mg complex or some native defect level.

YL in n-type GaN is often attributed to Ga vacancies and impurities, such as oxygen and carbon,[40] although it is not likely that these impurities are present in the samples through the growth process used. YL is also present in Mg-doped p-type porous GaN and can arise from a transition between the conduction band or shallow donors.[47] The YL has weak temperature dependence and is not found to vary considerably due to Mg incorporation into the lattice when compared to the undoped sample.

**3.5. Electrical Characterization.** Electrical characterization of the three types of porous GaN diodes is shown in Figure 7. Diodes comprising nonporous and porous GaN, and
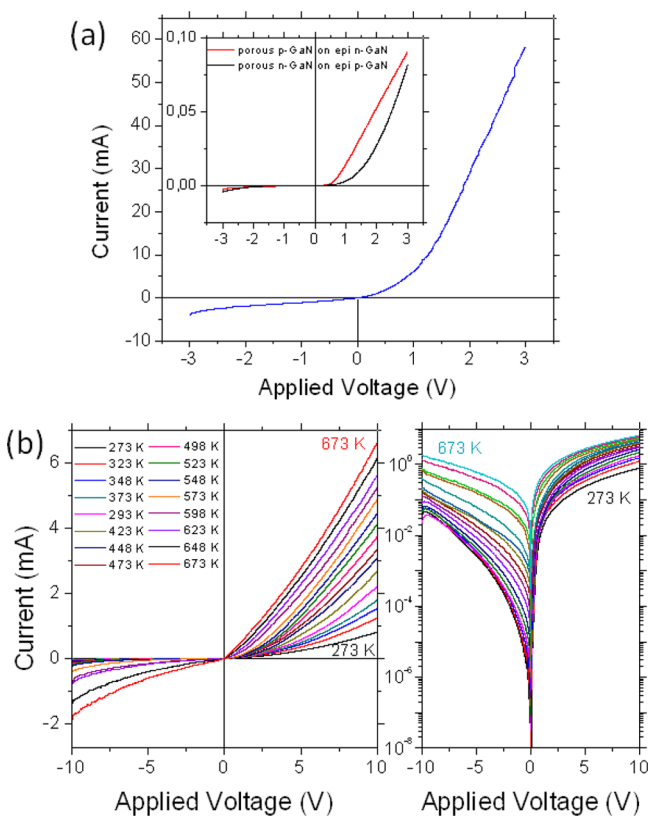


**Figure 7.** (a) $I-V$ curves of the fully porous diode. Inset shows the $I-V$ curves recorded for the porous n−p and porous p−n diodes. (b) $I-V$ curves of the porous n−p GaN diode recorded at $T = 298-673$ K.

also fully porous p−n GaN junction exhibited characteristic $I-V$ curves with strong rectification. Figure 7a shows the $I-V$ curve corresponding to the porous n−p diode. The high bias resistance turnover of the porous n-type GaN occurs just above 1 V. When the nonporous p-type GaN is positively biased, current flow through the p−n junction varies exponentially. The barrier to the exponential current increase is found to be much lower than the expected GaN diode response, that is, $E_g/q$. The turn-on voltage for this p−n junction lies in the range $\sim(E_g/4q)-(E_g/2q)$, that is, 0.5−0.68 V. In the case of the porous p−n and the fully porous GaN diode the turn-on voltage is found to be even lower, in the range $(E_g/4q)-(E_g/6q)$ (see Figure 7b). In all cases the diode behavior is confirmed and low reverse bias leakage currents were found for these

porous GaN structures. Moreover, the current at a fixed value of the forward voltage in the fully porous diode is found to be 3 orders of magnitude higher than that measured in the partially porous diodes.

The electron density for unintentionally doped porous n-type GaN is estimated to be $1.6 \times 10^{16}$ cm³.[31] The effective hole density for porous p-type GaN at 300 K is estimated using the effective hole and electron masses of wurzite GaN to be $\sim 9 \times 10^{18}$ cm⁻³.[32] Taking into account the values of donor and acceptor densities of nonporous n-type GaN and p-type GaN of $N_D = 10^{19}$ cm⁻³ and $N_A = 10^{18}$ cm⁻³, respectively, and the corresponding values mentioned above for porous n-type GaN and p-type GaN, we can estimate $V_B$ for the porous n−p diode as 0.72 V, for the porous p−n diode as 0.9 V, and for the totally porous diode as 0.71 V.

Based on these measurements, we should mention some important aspects for porous GaN p−n junctions. Microscopic characterization confirms well-defined interface between the porous and the nonporous GaN layers (see Figure 5), and thus, no significant tunnelling barrier exists either at the GaN−GaN interface or on the surface of the GaN/Ohmic contact. Also, microscopic characterization excludes any interfacial contaminants that would alter the effective barrier.

The barrier potentials are a function of the donor and acceptor densities, which also correlate to the n and p carrier concentrations assuming an abrupt junction formation (no concentration grading or midgap states etc.)

$$\left(\frac{N_D N_A}{n_i^2}\right) = \frac{n_n p_p}{n_p p_p} \tag{3}$$

The values for the epi-n and epi-p layers are nominally higher and have more accurate correlation between $N_D \sim n$, and $N_A \sim p$, such that the ratio is a lesser value for either of the semiporous junctions. Furthermore, for the porous GaN, the donor density ($N_D < n$).

The measurements were repeated from different points on several separate p−n junction diodes and they exhibited similar $I-V$ response, which augers well for high surface area diodes and parallel arrays of devices from completely porous p−n junctions over large areas.[48,49]

Figure 7b shows the $I-V$ curves recorded for the porous n−p diode at different temperatures ranging from 298 to 673 K, confirming that we are dealing with a rectifying diode in all p−n junctions. The forward and reverse bias currents of the diode increase with temperature, thus accounting for an increase of the number of charge carriers across the barrier height. The turn-on voltage for this junction is characteristically $\sim(E_g/4q)-(E_g/2q)$ at room temperature. With the increase of temperature, this low knee voltage is reduced even further consistent with a thermionic process with greater carrier velocities at higher temperatures. At the highest temperatures the high bias resistance turnover of the porous n−p diode occurs at very low potentials (~0.4−0.5 V), but the built-in potential

$$V_B = \frac{kT}{q}\ln\left(\frac{N_D N_A}{n_i^2}\right) \tag{4}$$

is overcome through tunneling. At all temperatures (at least to 673 K), the rectifying characteristics of the porous GaN diodes are preserved, and no breakdown voltage was observed even at 10 V at 673 K.

The fully porous GaN p−n junction diodes, and those comprising porous n- or p-type GaN on nonporous epilayers, exhibited stable rectification. Figure 8 shows current
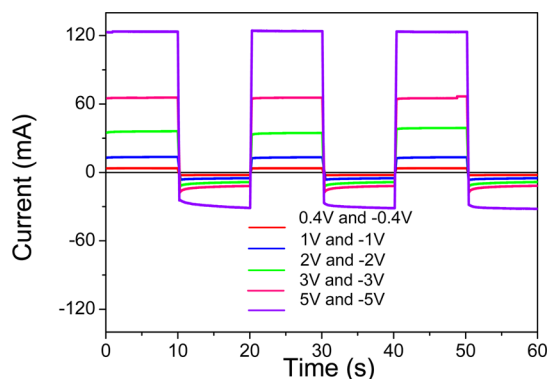


**Figure 8.** Rectifying characteristics of the fully porous diode at different voltages in the range 0.4−5 V.

rectification achieved at reverse bias and forward bias (>than knee voltage) recorded for the fully porous p−n diode (see Figure S2 in Supporting Information for current rectification in partially porous diodes) at a bias polarity switch frequency of 0.1 Hz at room temperature. The current−time ($I$−$t$) characteristics recorded at ±0.4 V does not show clear rectification behavior, since this voltage is below or on the limit of the turn-on voltage of the porous GaN diodes. At ± 1 V, ± 2 V, ± 3 V, and ±5 V voltages all diodes demonstrate rectifying behavior. The highest leakage voltage and the lowest rectification ratio is observed at ±5 V. Also, porous GaN diodes demonstrate very stable values of current with time at both, forward and reverse bias. The stability confirms that for porous p−n junctions using a single porous layer deposited on an epitaxial continuous GaN film, or from a porous layer grown on another porous layer, a remarkable stability in rectification is maintained. Porous GaN films can exhibit random porosity (compared to arrays of nanostructures), but their ease of deposition over large areas without dominating leakage currents is promising for wideband gap applications, including sensors.

## 4. CONCLUSIONS

Taken as a whole, the detailed investigation presented here demonstrates that completely porous high quality p−n junctions of porous n-type and porous p-type GaN can be grown over large areas by sequential chemical vapor deposition. The electrical and optical characteristics confirm high electronic quality GaN growth for porous layers when compared with nonporous epitaxially grown GaN, even when overgrown with opposite conduction type porous layer to form porous/nonporous p−n junction diodes. We believe this investigation can be extended to other III−N materials such as InN and AlN to span the visible spectrum, and as a route toward porous, graded index III−N materials as a basis for white light LEDs incorporating other color centers, or for reducing reflection losses and narrowing the output light cone for improved LED external quantum efficiencies. High surface area diodes by this route do not require complicated core−shell architectures in nanostructure arrays and may be viable routes to chemically stable wide bandgap (bio)sensors.

## ASSOCIATED CONTENT

### Supporting Information

Figure S1. High magnification SEM images of the porous structures observed on (a) n-type and (b) p-type GaN layers corresponding to the fully porous GaN diode. Figure S2. Rectification characteristics of the (a) porous n−p and (b) porous p−n diodes shown at different voltages. Table S1. Peak position and fwhm extracted from the rocking curves recorded for the (0004) reflection for the different layers of the diodes fabricated, and calculated relaxation of the different porous layers calculated according to eq 1. This material is available free of charge via the Internet at http://pubs.acs.org.

## AUTHOR INFORMATION

### Corresponding Authors
* E-mail: joanjosep.carvajal@urv.cat.
*E-mail: c.odwyer@ucc.ie.

### Author Contributions

The manuscript was written through contributions of all authors. All authors have given approval to the final version of the manuscript.

### Notes

The authors declare no competing financial interest.

## ACKNOWLEDGMENTS

## REFERENCES

(1) *Anual Energy Review 2011*; U.S. Energy Information Administration: Washington, DC, 2011; DOE/EIA-0384.

(2) Nakamura, S.; Pearton, S.; Fasol, G. *The Blue Laser Diode: The Complete Story*, 1st ed; Springer-Verlag: Berlin, 2000.

(3) Hwang, J. M.; Hung, W. H.; Hwang, H. L. Efficiency Enhancement of Light Extraction in LED With a Nano-Porous GaP Surface. *IEEE Photonics Technol. Lett.* **2008**, *20*, 608−610.

(4) Wierer, J. J.; David, A.; Megens, M. M. III-Nitride Photonic-Crystal Light-Emitting Diodes with High Extraction Efficiency. *Nat. Photonics* **2009**, *3*, 163−169.

(5) Kim, T. K.; Kim, S. H.; Yang, S. S.; Son, J. K.; Lee, K. H.; Hong, Y. G.; Shim, K. H.; Yang, J. W.; Lim, K. Y.; Bae, S. J.; Yang, G. M. GaN-based Light-Emitting Diode with Textured Indium Tin Oxide Transparent Layer Coated with $Al_2O_3$ Powder. *Appl. Phys. Lett.* **2009**, *94*, 161107.

(6) Lee, C.-H.; Yoo, J.; Hong, Y. J.; Cho, J.; Kim, Y.-J.; Jeon, S.-R.; Baek, J. H.; Yi, G.-C. GaN/In$_{1−x}$Ga$_x$N/GaN/ZnO Nanoarchitecture Light Emitting Diode Microarrays. *Appl. Phys. Lett.* **2009**, *94*, 213101.

(7) Liu, D.-S.; Lin, T.-W.; Huang, B.-W.; Juang, F.-S.; Lei, P.-H.; Hu, C.-Z. Light-Extraction Enhancement in GaN-based Light-Emitting Diodes Using Grade-Refractive-Index Amorphous Titanium Oxide Films with Porous Structures. *Appl. Phys. Lett.* **2009**, *94*, 143502.

(8) Ryu, S.-W.; Park, J.; Oh, J.-K.; Long, D. H.; Kwon, K.-W.; Kim, Y.-H.; Lee, J. K.; Kim, J. H. Analysis of Improved Efficiency of InGaN Light-Emitting Diode with Bottom Photonic Crystal Fabricated by Anodized Aluminum Oxide. *Adv. Funct. Mater.* **2009**, *19*, 1650−1655.

17962

dx.doi.org/10.1021/am504786b | *ACS Appl. Mater. Interfaces* 2014, 6, 17954−17964

(9) Lo, M. H.; Tu, P. M.; Wang, C. H.; Hung, C. W.; Hsu, S. C.; Cheng, Y. J.; Kuo, H. C.; Zan, H. W.; Wang, S. C.; Chang, C. Y.; Huang, S. C. High Efficiency Light Emitting Diode with Anisotropically Etched GaN-sapphire Interface. *Appl. Phys. Lett.* **2009**, *95*, 041109.

(10) Song, Y. M.; Choi, E. S.; Park, G. C.; Park, C. Y.; Jang, S. J.; Lee, Y. T. Disordered Antireflective Nanostructures on GaN-based Light-Emitting Diodes Using Ag Nanoparticles for Improved Light Extraction Efficiency. *Appl. Phys. Lett.* **2010**, *97*, 093110.

(11) Cho, C.-Y.; Kang, S.-E.; Kim, K. S.; Lee, S.-J.; Choi, Y.-S.; Han, S.-H.; Jung, G.-Y.; Park, S.-J. Enhanced Light Extraction in Light-Emitting Diodes with Photonic Crystal Structure Selectively Grown on p-GaN. *Appl. Phys. Lett.* **2010**, *96*, 181110.

(12) Chhajed, S.; Lee, W.; Cho, J.; Schubert, E. F.; Kim, J. K. Strong Light Extraction Enhancement in GaInN Light-Emitting Diodes by Using Self-Organized Nanoscale Patterning of p-Type GaN. *Appl. Phys. Lett.* **2011**, *98*, 071102.

(13) Fu, X. X.; Zhang, B.; Kang, X. N.; Deng, J. J.; Xiong, C.; Dai, T.; Jiang, X. Z.; Yu, T. J.; Chen, Z. Z.; Zhang, G. Y. GaN-based Light-Emitting Diodes with Photonic Crystal Structures Fabricated by Porous Anodic Alumina Template. *Opt. Express* **2011**, *19*, A1104−A1108.

(14) Liu, D. S.; Lin, T. W.; Huang, B. W.; Juang, F. S.; Lei, P. H.; Hu, C. Z. Light-Extraction Enhancement in GaN-based Light-Emitting Diodes Using Grade-Refractive-Index Amorphous Titanium Oxide Films with Porous Structures. *Appl. Phys. Lett.* **2009**, *94*, 143502.

(15) O'Dwyer, C.; Szachowicz, M.; Visimberga, G.; Lavayen, V.; Newcomb, S. B.; Sotomayor Torres, C. M. Bottom-up Growth of Fully Transparent Contact Layers of Indium Tin Oxide Nanowires for Light Emitting Devices. *Nat. Nanotechnol.* **2009**, *4*, 239−244.

(16) O'Dwyer, C.; Sotomayor Torres, C. M. Epitaxial Growth of an Antireflective, Conductive, Graded Index ITO Nanowire Layer. *Front. Phys.* **2013**, *1*, 18.

(17) Kim, T. K.; Kim, S. H.; Yang, S. S.; Son, J. K.; Lee, K. H.; Hong, Y. G.; Shim, K. H.; Yang, J. W.; Lim, K. Y.; Bae, S. J. GaN-Based Light-Emitting Diode with Textured Indium Tin Oxide Transparent Layer Coated with $Al_2O_3$ Powder. *Appl. Phys. Lett.* **2009**, *94*, 161107.

(18) Vial, J. C.; Bsiesy, A.; Gaspard, F.; Herino, R.; Ligeon, M.; Müller, F.; Romestain, R.; Macfarlane, R. M. Mechanisms of Visible-Light Emission from Electro-Oxidized Porous Silicon. *Phys. Rev. B* **1992**, *45*, 13171−14176.

(19) Graham, A. H. D.; Bowen, C. R.; Robbins, J.; Lalev, G.; Marken, F.; Taylor, J. Nanostructured Electrodes for Biocompatible CMOS Integrated Circuits. *Sens. Actuators, B* **2010**, *147*, 697−706.

(20) Valerini, D.; Cretì, A.; Caricato, A. P.; Lomascolo, M.; Rella, R.; Martino, M. Optical Gas Sensing Through Nanostructured ZnO Films with Different Morphologies. *Sens. Actuators, B* **2010**, *145*, 167−173.

(21) Pearton, S. J.; Ren, F. GaN Electronics. *Adv. Mater.* **2000**, *12*, 1571−1580.

(22) Fan, Z.; Razavi, H.; Do, J.; Moriwaki, A.; Ergen, O.; Chueh, Y.-L.; Leu, P. W.; Ho, J. C.; Takahashi, T.; Reichertz, L. A.; Neale, S.; Yu, K.; Wu, M.; Ager, J. W.; Javey, A. Three-Dimensional Nanopillar-Array Photovoltaics on Low-Cost and Flexible Substrates. *Nat. Mater.* **2009**, *8*, 648−653.

(23) Anglin, E. J.; Cheng, L.; Freeman, W. R.; Sailor, M. J. Porous Silicon in Drug Delivery Devices and Materials. *Adv. Drug Delivery Rev.* **2008**, *60*, 1266−1277.

(24) Jiménez-Cadena, G.; Riu, J.; Rius, F. X. Gas Sensors Based on Nanostructured Materials. *Analyst* **2007**, *132*, 1083−1099.

(25) Bacci, N.; Diligenti, A.; Barillaro, G. Fabrication, Electrical Characterization, and Modeling of Fully-Porous p−n Junctions. *J. Appl. Phys.* **2011**, *110*, 036106.

(26) Sun, W.; Kherani, N. P.; Hirschman, K. D.; Gadeken, L. L.; Fauchet, P. M. A Three-Dimensional Porous Silicon p−n Diode for Betavoltaics and Photovoltaics. *Adv. Mater.* **2005**, *17*, 1230−1233.

(27) Luque, A.; Muati, A. Increasing the Efficiency of Ideal Solar Cells by Photon Induced Transitions at Intermediate Levels. *Phys. Rev. Lett.* **1997**, *78*, 5014−5017.

(28) Ho, C. H.; Lien, D. H.; Chang, H. C.; Lin, C. A.; Kang, C. F.; Hsing, M. K.; Lai, K. Y.; He, J. H. Hierarchical Structures Consisting of $SiO_2$ Nanorods and p-GaN Microdomes for Efficiently Harvesting Solar Energy for InGaN Quantum Well Photovoltaic Cells. *Nanoscale* **2012**, *4*, 7346−7349.

(29) Carvajal, J. J.; Rojo, J. C. Morphology Control in As-Grown GaN Nanoporous Particles. *Cryst. Growth Des.* **2009**, *9*, 320−326.

(30) Carvajal, J. J.; Bilousov, O. V.; Drouin, D.; Aguiló, M.; Díaz, F.; Rojo, J. C. Chemical Vapor Deposition of Porous GaN Particles on Silicon. *Microsc. Microanal.* **2012**, *18*, 905−911.

(31) Bilousov, O. V.; Carvajal, J. J.; Drouin, D.; Mateos, X.; Díaz, F.; Aguiló, M.; O'Dwyer, C. Reduced Workfunction Intermetallic Seed Layers Allow Growth of Porous n-GaN and Low Resistivity, Ohmic Electron Transport. *ACS Appl. Mater. Interfaces* **2012**, *4*, 6927−6934.

(32) Bilousov, O. V.; Geaney, H.; Carvajal, J. J.; Zubialevich, V. Z.; Parbrook, P. J.; Giguère, A.; Drouin, D.; Díaz, F.; Aguiló, M.; O'Dwyer, C. Fabrication of p-Type Porous GaN on Silicon and Epitaxial GaN. *Appl. Phys. Lett.* **2013**, *103*, 112103.

(33) Götz, W.; Johnson, N. M.; Walker, J.; Bour, D. P.; Street, R. A. Activation of Acceptors in Mg-Doped GaN Grown by Metalorganic Chemical Vapor Deposition. *Appl. Phys. Lett.* **1996**, *68*, 667−669.

(34) Pearton, S. J.; Wilson, R. G.; Zavada, J. M.; Han, J.; Shul, R. J. Thermal Stability of $^2$H-Implanted n- and p-Type GaN. *Appl. Phys. Lett.* **1998**, *73*, 1877−1879.

(35) Görgens, L.; Ambacher, O.; Stutzmann, M.; Miskys, C.; Scholz, F.; Off, J. Characterization of InGaN Thin Films Using High-Resolution X-ray Diffraction. *Appl. Phys. Lett.* **2000**, *76*, 577−579.

(36) Mynbaeva, M.; Titkov, A.; Kryganovskii, A.; Ratnikov, V.; Mynbaev, K.; Huhtinen, H.; Laiho, R.; Dmitriev, V. Structural Characterization and Strain Relaxation in Porous GaN Layers. *Appl. Phys. Lett.* **2000**, *76*, 1113−1115.

(37) Dassonneville, S.; Amokrane, A.; Sieber, B.; Farvacque, J.-L.; Beaumont, B.; Gibart, P. Luminescence of Epitaxial GaN Laterally Overgrown on (0001) Sapphire Substrate: Spectroscopic Characterization and Dislocation Contrasts. *J. Appl. Phys.* **2001**, *89*, 3736−3743.

(38) Sun, X. L.; Goss, S. H.; Brillson, L. J.; Look, D. C.; Molnar, R. J. Depth-dependent Investigation of Defects and Impurity Doping in GaN/Sapphire Using Scanning Electron Microscopy and Cathodoluminescence Spectroscopy. *J. Appl. Phys.* **2002**, *91*, 6729−6738.

(39) Zaldivar, M. H.; Fernández, P.; Piqueras, J. Luminescence from Growth Topographic Features in GaN:Si Films. *J. Appl. Phys.* **1998**, *83*, 462−465.

(40) Neugebauer, J.; van de Walle, C. G. Gallium Vacancies and the Yellow Luminescence in GaN. *Appl. Phys. Lett.* **1996**, *69*, 503−505.

(41) Myoung, J.-M.; Shim, K.-H.; Kim, S. Depth-Resolved Cathodoluminescence of III−V Nitride Films Grown by Plasma-Assisted Molecular Beam Epitaxy. *Jpn. J. Appl. Phys.* **2001**, *40*, 476−479.

(42) Bertram, F.; Christen, J.; Schmidt, M.; Topf, M.; Koymov, S.; Fischer, S.; Meyer, B. Strong Morphological Dependence of Luminescence Efficiency and Emission Wavelength in Hexagonal GaN Crystallites Directly Imaged by Scanning Cathodoluminescence Microscopy. *Mater. Sci. Eng., B* **1997**, *50*, 165−169.

(43) Shan, W.; Schmidt, T. J.; Yang, X. H.; Hwang, S. J.; Song, J. J.; Goldenberg, B. Temperature Dependence of Interband Transitions in GaN Grown by Metalorganic Chemical Vapor Deposition. *Appl. Phys. Lett.* **1995**, *66*, 985−987.

(44) Jain, S. C.; Willander, M.; Narayan, J.; Overstraeten, R. V. III−Nitrides: Growth, Characterization, and Properties. *J. Appl. Phys.* **2000**, *87*, 965−1006.

(45) Eckey, L.; Holst, J.-C.; Maxim, P.; Heitz, R.; Hoffmann, A.; Broser, I.; Meyer, B. K.; Wetzel, C.; Mokhov, E. N.; Baranov, P. G. Dynamics of Bound-Exciton Luminescences from Epitaxial GaN. *Appl. Phys. Lett.* **1996**, *68*, 415−417.

(46) Reshchikov, M. A.; Morkoç, H. Luminescence Properties of Defects in GaN. *J. Appl. Phys.* **2005**, *97*, 061301.

(47) Gelhausen, O.; Klein, H. N.; Phillips, M. R.; Goldys, E. M. Low-energy Electron-Beam Irradiation and Yellow Luminescence in Activated Mg-Doped GaN. *Appl. Phys. Lett.* **2003**, *83*, 3293−3295.

(48) Huang, Y.; Duan, X.; Cui, Y.; Lieber, C. M. Gallium Nitride Nanowire Nanodevices. *Nano Lett.* **2002**, *2*, 101−104.

(49) Duan, X.; Lieber, C. M. Laser-Assisted Catalytic Growth of Single Crystal GaN Nanowires. *J. Am. Chem. Soc. 122*, 188−189.

17964

dx.doi.org/10.1021/am504786b | *ACS Appl. Mater. Interfaces* 2014, 6, 17954−17964